Irene Aliatis[a], Luciana Mantovani [a], Danilo Bersani [a], G. Diego Gatta [b], Mario Tribaudino [a], Pier Paolo Lottici[a]

High-Pressure Raman spectroscopy on low albite

[a] *Università di Parma, Dipartimento di Fisica e Scienze della Terra, Parco Area delle Scienze 7/A, 43124 Parma, Italy.*
[b] *Università degli Studi di Milano, Dipartimento di Scienze della Terra, via Botticelli 23, 20133 Milano, Italy.*
Corresponding author: E-mail: irene.aliatis@difest.unipr.it; +39 0521 905238

Abstract

The pressure-dependence of the Raman spectrum of low albite, $NaAlSi_3O_8$, has been investigated from 0.0001 to 10.4 GPa, at room temperature, on a single crystal compressed hydrostatically in a diamond-anvil cell. The Raman vibrational features move to higher wavenumbers ν_i with increasing pressure, due to the decrease of the unit-cell volume corresponding to a drastic shrinkage of the framework. The slopes $\Delta\nu_i/\Delta P$ of the four investigated bending modes (*i.e.*, at 478, 507, 578 and 815 cm^{-1}, at 0.0001 GPa) show evident changes at ~6.5 GPa and at ~8.5 GPa. This behaviour may be ascribed, in the absence of phase transitions, to the evolution of the compressional mechanisms at the atomic scale found in previous high-pressure studies on albite (mainly by X-ray diffraction), through a model based on tilts of rigid tetrahedra. The Raman data of this study allowed also to bracket the pressure range in which the occurrence of the first change in the compressional behaviour was found by X-ray diffraction. A comparative analysis between the main *P*-induced deformation mechanisms, based on previous X-ray structure investigations, and the present Raman results is carried out.

Keywords Feldspars, low albite, high-pressure Raman spectroscopy, compressional behaviour.

Acknowledgments

This work was supported by the Italian Ministry of Education (MIUR), grant numbers 2010EARRRZ_005 and 2008SPZ743 which is gratefully acknowledged. We also acknowledge the generous support to the discussion of R. J. Angel.

Introduction

The compressional behaviour of feldspars has been deeply studied in order to understand the mechanisms that control the elastic properties of this abundant class of minerals of the Earth's crust (~ 60 wt%) (*e.g.* Angel 1992; Daniel et al. 1995; Daniel et al. 1997; Downs et al. 1999; Angel 2004; Benusa et al. 2005; Angel et al. 2012; Angel et al. 2013). The pressure range over which feldspars are thermodynamically stable is limited to 1 GPa in geological environments (Downs et al. 1994; Benusa et al. 2005; Carpenter 2006), and they become metastable at higher pressures. Nevertheless, compressional studies at high pressures are needed to provide more accurate data on the thermodynamic properties of these minerals, and to interpret the deformation changes in the framework, eventually leading to amorphization and to

diaplectic glasses with feldspathic composition, as maskelenyte, which are commonly found in natural meteorites (Velde et al. 1989; Fritz et al. 2005).

Feldspars are significantly stiffer than other open-framework silicates, such as quartz (Angel et al. 1997) or zeolites (Gatta and Lee 2014) but, among rock-forming minerals, they are softer than other rock-forming silicate, *e.g.* olivine and pyroxenes (Angel 2004). Among natural feldspars, the thermoelastic behaviour of low albite (ideally $NaAlSi_3O_8$) has deserved special attention: low albite shows significantly higher thermal expansion than other plagioclases, almost twice than anorthite (Tribaudino et al. 2010), lower Einstein temperature and more anisotropic thermal deformation (Tribaudino et al. 2011). Moreover, the unit-cell volume of albite shows a non-linear trend at almost any temperature, unlike other plagioclases (Tribaudino et al. 2010; Tribaudino et al. 2011). At high pressure, recent determinations of the equation of state (EoS) of plagioclases (Angel 2004) revealed that low albite shows unusual features (Downs et al. 1994; Benusa et al. 2005): it remains triclinic with $C\bar{1}$ symmetry at least up to 9.4 GPa and no phase transition occurs (Benusa et al. 2005), although the unit-cell volume and axial parameters *vs.* *P* show a change at $P > 4$ GPa, ascribable to a change of the compressional mechanisms at the atomic scale. The first *P*-derivative of the bulk modulus, obtained by an isothermal Birch-Murnaghan EoS fit (Birch 1966), has values $K' = \partial K/\partial P > 4$ below 4 GPa, whereas at higher pressure $K' < 4$, as observed in the anorthite-richer plagioclases (with An content higher than 30%, Angel 2004). The closing-up of the crankshaft chains is the dominant compression mechanism and is responsible for the extreme anisotropy of compression that is typical for all feldspars (Angel et al. 1988; Angel 2004). Albite reveals a more complex behaviour than other feldspars (Benusa et al. 2005). Two secondary compressional mechanisms act at different pressures: i) below 4 GPa, the closing-up of the crankshaft chains is the major mechanism, without rotation of T_1 tetrahedra, in addition to the shear of four-membered rings; ii) above 4-5 GPa, T_1 tetrahedra rotate around [001] direction and albite becomes softer, similarly to what is observed in plagioclase at lower pressures (Angel 2004); iii) above 8 GPa, a severe softening of the structure as a whole occurs, coupled with an expansion along some directions (*e.g.*, [110]). At $P > 8$ GPa, the smallest T-O_C(o)-T angle decreases to a value of ~113°, which represents an extreme limit for Al-O-Si bonds, because it enables a Al-Si distance of ~2.8 Å (Benusa et al. 2005). Calculation of the strain tensor (Ohashi and Burnham 1973) from the unit-cell parameters showed that the direction of maximum compression is close to the (100) plane normal, *i.e.*, along the extension direction of the crankshaft chains, and that this direction accommodates about the 65% of the volume compression of the framework.

In this paper, the results of an in-situ high-pressure Raman spectroscopic study on a single-crystal of low albite are reported, in order to describe the high-pressure vibrational behaviour of this feldspar, compared with its elastic properties as determined by in-situ high-pressure X-ray diffraction experiments (Downs et al. 1994; Benusa et al. 2005). As far as we know, this is the first experiment in which the evolution of the single-crystal Raman spectrum of albite with pressure is reported.

Experimental method

The high-pressure Raman spectroscopy experiment was performed on a single crystal of low albite from Minas Gerais (Brazil) [a = 8.1395(5) Å, b = 12.7838(7) Å, c = 7.1597(6) Å, α = 94.242(6)°, β = 116.590(7)°, γ = 87.674(5)°, V = 664.35(9) Å^3, space group $C\bar{1}$]. EPMA-EDS indicate an almost end-member composition, with K_2O and CaO

concentrations of 0.32 and 0.19 wt%, respectively. Further details pertaining to the crystal-chemical characterization of the sample (*e.g.*, chemical analysis protocol, unit-cell parameters measurement and single-crystal structure refinement procedure) can be found in Aliatis et al. (2015).

An ETH-type diamond anvil cell (DAC), designed by Miletich et al. (2000), was used for the high-pressure Raman experiment. Stainless-steel T301 foil, 250 μm thick, pre-indented to a thickness of about 100 μm and with a 300 μm hole obtained by electro-spark erosion, was used as a gasket. Type-II diamonds were used as anvils (culet diameter: 600 μm). A single crystal of low albite (120 x 100 x 20 μm^3) was placed in the gasket hole along with some ruby chips for pressure measurements by the ruby-fluorescence method (precision of ± 0.05 GPa) (Mao et al. 1986). Methanol:ethanol = 4:1 mixture was used as hydrostatic pressure-transmitting fluid (Angel et al. 2007).

Raman spectra were collected in the pressure range 0.0001 - 10.4(5) GPa (16 measurements in compression and 6 in decompression) using an Olympus BX40 microscope attached to a Jobin Yvon Horiba LabRam confocal Raman spectrometer, equipped with a charge-coupled detector (CCD). The sample was excited by a continuous-wave single frequency Nd:YAG blue laser at 473.1 nm end-pumped by a laser diode. The laser beam was focused on the sample with a spot diameter of nearly 1 μm (50x ultra long working distance objective, NA = 0.55), using a confocal aperture of 150 μm. The spectral resolution was about 3.5 cm^{-1}. Unpolarized Raman spectra were collected in backscattered geometry in the spectral range 100-2000 cm^{-1}, with 60-90 s counting times and 6-10 accumulations.

The (010) cleavage face of the albite crystal was set as much as possible parallel to the culet face of the anvil. The same configuration was maintained for all the spectra. Before each measurement of the Raman spectrum of the sample and of the fluorescence spectrum of ruby, the spectrometer was calibrated using the emission lines of a spectroscopic Zn lamp in the two different spectral ranges. In addition, all spectra were collected at least 20 min after increasing the pressure. The positions of the Raman bands were determined, with accuracy better than 0.5 cm^{-1}, after a polynomial baseline subtraction, by pseudo-Voigt deconvolution procedure (LABSPEC 5.78.24 software package, Jobin Yvon Horiba).

Results

Some representative Raman spectra of low albite collected in compression and decompression mode are shown in Fig. 1. Twenty-five modes, out of the 39 A_g modes expected by factor group analysis (Aliatis et al. 2015) were observed with the sample inside the DAC. The useful data were in the spectral range up to 850 cm^{-1}, due to the intense Raman bands at 880 and 1000 cm^{-1} of the pressure-fluid (*i.e.*, methanol or ethanol) and to the strong diamond peak at 1332 cm^{-1}. At high pressure a general deterioration of the Raman signal due to band overlapping was observed. As an example, the characteristic peaks at 478 and 507 cm^{-1} become a single unresolved band at $P > 8$ GPa, but they split again in decompression.

The major features of the Raman spectra collected at room conditions are preserved up to the highest pressure, with no evidence of amorphization effects. Some of the weakest Raman bands of low albite disappear with increasing pressure, especially at low wavenumbers: the number of the observable Raman modes below 250 cm^{-1} decreases from 7 to 4 at 2.9 GPa, and the *P*-evolution of the Raman features in this spectral range cannot be determined unambiguously.

A shift towards higher wavenumbers is observed for all Raman modes during compression, an effect completely reversible in decompression. The distances between the building units forming the albite framework (*i.e.*, Si or Al tetrahedra) decrease with increasing pressure and the stronger electrostatic repulsion causes the observed blue-shifts.

In the following, the wavenumbers used to label the investigated Raman bands are those found in the Raman spectrum at room *T*, *P*. The pressure-induced evolution of six selected (well observable) Raman bands at 149-290-48-507-578-815 cm^{-1}, along with the linear fits to their $\upsilon_i(P)$ curves, are shown in Fig. 2. The wavenumber blue shifts, within the full *P*-range investigated, are: $\Delta\upsilon_{149} = 26.0\ cm^{-1}$, $\Delta\upsilon_{290} = 15.7\ cm^{-1}$, $\Delta\upsilon_{478} = 29.1\ cm^{-1}$, $\Delta\upsilon_{507} = 16.2\ cm^{-1}$, $\Delta\upsilon_{578} = 4.2\ cm^{-1}$, and $\Delta\upsilon_{815} = 17.3\ cm^{-1}$.

Excluding the Raman band at 149 cm^{-1}, which displays a constant $\Delta\upsilon/\Delta P$ slope over the entire *P*-range, variations of the $\Delta\upsilon_i/\Delta P$ slopes are observed for the studied modes (see Table 1). This suggests different compressional mechanisms for the building units involved in each mode. The modes involving mainly Na (*e.g.*, 149 cm^{-1}, Aliatis et al 2015) show the most pronounced changes in slope with pressure, consistent with the clue that Na atoms are just 'pushed around' by the framework and that the cavity is rapidly compressed. A common feature of the $\upsilon_i(P)$ curves is an apparent discontinuity at ~ 6.5 GPa. Raman data suggest, therefore, that the internal structural rearrangements occur in a sharp pressure interval, at about 6.5 GPa and not spread out from 4 to 8 GPa as suggested by previous X-rays studies on elasticity (Benusa et al. 2005). This behaviour cannot be ascribed to a phase transition (as it can be ruled out on the basis of the X-ray data), it is rather the effect of a change in the compressional mechanisms at the atomic scale, with a resulting change of the elastic behaviour. In addition, whereas most modes evolve smoothly for $P > 7$ GPa, the high-frequency mode at 815 cm^{-1} shows another discontinuity in $\upsilon_{815}(P)$ at $P \sim 8.5$ GPa.

Discussion

Interesting correspondences can be found if the in-situ high-pressure Raman results here reported and the structural data from literature are compared. Looking at the pressure-evolution of the T-O-T bond angles and of the O-O-O ring angles, based on the structure refinements, as given by Benusa et al. (2005), a discontinuity at $P \sim 6$ GPa is detected. In particular, the most evident structural rearrangement reflects the reduction in the T-O_B(o)-T and T-O_C(o)-T bond angles, which results in the closing-up of the crankshaft chains and in the shear of the four-membered rings of tetrahedra. The shear causes the narrowing of the channels which is responsible of the softness along the (100) plane normal, as observed in all feldspars (Downs et al. 1994; Angel 2004; Benusa et al. 2005). Angel et al. (2012) showed that all the essential features of the structures (*i.e.*, unit-cell parameters and volumes, their expansion and compression induced by changes in pressure, temperature, and composition) are generated by tetrahedral tilting, and that the fundamental reason for feldspars anisotropy lies in the topology of the tetrahedral framework. In particular, four tilts are allowed in a ring of four corner-linked tetrahedra with point symmetry 2: #1 the rotation of T_1 tetrahedra around the O_B-O_D edge; #2 rotation of T_2 tetrahedra around the O_B-O_D edge; #3 mutual rotation of the T_2 by equal but opposite amounts around a^*; #4 shear of the ring within the (010) plane. In triclinic feldspars, there are four non-equivalent tetrahedra, so four individual tilts of the tetrahedra with respect to the ring: tilt #1 will be split in T_1(o) and T_1(m) tilts, and tilt #2 in T_2(o) and T_2(m) tilts. The O-O repulsions control the values of these tilts and, therefore, the anisotropy of the structure, because tilts maximize the shortest O-O distances in the structure (Angel et al. 2012; Angel et al. 2013). Therefore, considering the structural changes in terms of tilts of rigid tetrahedra, the variation in the tilting angles are expected to

be relate especially with the framework bending modes (*i.e.*, the Raman modes at 478, 507, 578 and 815 cm^{-1}, Aliatis et al. 2015).

The pressure-induced evolution of tilt angles in triclinic structures is shown in Fig. 3. They have been recalculated from the experimental data of Benusa et al. (2005) and Downs et al. (1994), using the definition and the calculations reported in Angel et al. (2012). It is evident that the rate in the variation of all tilts changes significantly at 6 GPa, in good agreement with our Raman data of this study. In Fig. 4, the correlation between the change in O-O-O angles and tilt #4 (*i.e.*, shear of the ring) is shown. Tilts do not include the internal deformation of the tetrahedra, because they are only a measure of the response of the structure interpreted in terms of non-deformable tetrahedra, so they do not explain the further change at $P > 8.5$ GPa.

The Raman mode at 478 cm^{-1} shows the most pronounced Raman shift between 0.0001 and 6.5 GPa ($\Delta\upsilon_{478} = 29.1$ cm^{-1}, Table 1). Comparing the vibrational patterns corresponding to the Raman features at 478, 507, 578 and 815 cm^{-1}, it appears, especially in the *ab* projection (Fig. 5), that the mode at 478 cm^{-1} squeezes the cage inwards, whereas the modes at higher wavenumbers stretch the cage outwards. Changes in T-O-T and O-O-O angles result in the narrowing of the tetrahedral cages, which causes an increase in the Coulomb repulsion between atoms: the atomic pattern of the mode at 478 cm^{-1} may explain its largest wavenumber increase with pressure.

At $P > 6.5$ GPa, the Raman band at 507 cm^{-1} exhibits the steepest $\Delta\upsilon/\Delta P$ and the slope of the 578 cm^{-1} mode changes its sign (see Table 1), suggesting a relevant structural rearrangement.

In addition to the 6.5 GPa discontinuity, the mode at 815 cm^{-1} shows a further abrupt change in $\Delta\upsilon/\Delta P$ at about 8.5 GPa. As reported in Aliatis et al. (2015), this mode has a significant contribution from Si-O stretching vibrations and may be affected by variation of the internal geometry of the TO_4 tetrahedra. The discontinuity at 8.5 GPa could mirror the severe softening of the structure observed at $P > 8$ GPa by Benusa et al. (2005).

The discontinuity at 6.5 GPa may be noticed, even if at a lesser extent, also by the Raman mode at 290 cm^{-1}, which consists mainly of rotations of the tetrahedra (Aliatis et al. 2015).

The wavenumber of the Raman mode at ~ 149 cm^{-1} changes linearly over the entire investigated pressure range. This mode is related mostly to the Na atoms vibrations, in particular to Na translations within the tetrahedral cage (Aliatis et al. 2015). As the Na atoms are just 'pushed around' (Downs et al. 1994; Benusa et al. 2005), and the cavity tends to be rapidly compressed, a significant change with pressure is expected. Na atom does not change its coordination number within the *P*-range investigated, despite the significant decrease in the Na-O distances; this in contrast to microcline, where the K site increases its coordination number by bonding the additional $O_B(m)$ atom as the framework is compressed (Downs et al. 1999). In this respect, the behaviour of the extra-framework population with increasing pressure in albite is similar to that observed in other open-framework silicates (*e.g.*, some zeolites or feldspathoids, Gatta 2008; Gatta 2010; Gatta and Lotti 2016).

Changes in peak linewidth are not significant (*i.e.*, maximum increase of about 2-2.5 cm^{-1} in the investigated pressure range), confirming that the experiment was conducted under hydrostatic conditions and no evidence of *P*-induced amorphization occurs up to the maximum pressure achieved.

Conclusions

To the best of our knowledge, this is the first study in which the evolution of the Raman active modes of low albite has been investigated by an in-situ experiment up to 10.4 GPa. Our experimental findings can be summarized as follows: the six investigated Raman modes (*i.e.*, 149, 290, 478, 507, 578, 815 cm^{-1} at 0.0001 GPa) show a smooth evolution (stiffening) from room pressure to about 6 GPa and, excluding the mode involving Na atoms (*i.e.*, 149 cm^{-1}), a significant change in their vibrational behaviour occurs at $P \sim 6.5$ GPa: this allows localizing the first change in the compressional behaviour of albite previously found by X-ray diffraction in a large P range (*i.e.*, 4-8 GPa). A further change at about 8.5 GPa of the mode at 815 cm^{-1} confirms a second rearrangement of the structure, including the compression and severe distortion of the tetrahedra, observed by X-ray diffraction at $P > 8$ GPa.

191 **References**

192 Aliatis I, Lambruschi E, Mantovani L, Bersani D, Andò S, Gatta GD, Gentile P, Salvioli-Mariani E, Prencipe M,
193 Tribaudino M, Lottici PP (2015) A comparison between ab initio calculated and measured Raman spectrum of
194 triclinic albite (NaAlSi3O8). J Raman Spectrosc 46: 501–508

195 Angel RJ (1992) Order-disorder and the high-pressure P1-I1 transition in anorthite. Am Mineral 77:923–929.

196 Angel RJ (2004) Equations of state of Plagioclase Feldspars. Contrib to Mineral Petrol 146:506–512.

197 Angel RJ, Allan DR, Miletich R, Finger LW (1997) The use of quartz as an internal pressure standard in high-pressure
198 crystallography. J Appl Crystallogr 30:461–466.

199 Angel RJ, Bujak M, Zhao J, Gatta GD, Jacobsen SD (2007) Effective hydrostatic limits of pressure media for high-
200 pressure crystallographic studies. J Appl Crystallogr 40:26–32.

201 Angel RJ, Hazen RM, McCormick TC, Prewitt CT, Smith JR (1988) Comparative compressibility of end-member
202 feldspars. Phys Chem Miner 15:313–318.

203 Angel RJ, Ross NL, Zhao J, Sochalski-Kolbus LM, Kruger H, Schmidt BC (2013) Structural controls on the anisotropy
204 of tetrahedral framework: the example of monoclinic feldspars. Eur J Mineral 25:597–614.

205 Angel RJ, Sochalski-Kolbus LM, Tribaudino M (2012) Tilts and tetrahedra: The origin of the anisotropy of feldspars.
206 Am Mineral 97:765–778.

207 Benusa MD, Angel RJRJ, Ross NL (2005) Compression of albite, $NaAlSi_3O_8$. Am Mineral 90:1115–1120.

208 Birch F (1966) Compressibility, elastic constants. In: Clark SP (ed) Handbook of physical constants. Geol. Soc. Am.
209 Mem., pp 97–174

210 Carpenter MA (2006) Elastic properties of minerals and the influence of phase transitions. American Mineralogist
211 91:229–246.

212 Daniel I, Gillet P, Ghose S (1995) A new high-pressure phase transition in anorthite ($CaAl_2Si_20_8$) revealed by Raman
213 spectroscopy. Am Mineral 80:645–648.

214 Daniel I, Gillet P, McMillan PF, Wolf G,Verhelst MA (1997) High-pressure behavior of anorthite: Compression and
215 amorphization. J Geophys Res 102:10313.

216 Downs RT, Hazen RM, Finger LW (1994) The high-pressure crystal chemistry of low albite and the origin of the
217 pressure dependency of Al-Si ordering. Am Mineral 79:1042–1052.

218 Downs RT, Yang H, Hazen RM, Finger LW, Prewitt CT (1999) Compressibility mechanisms of alkali feldspars:
219 New data from reedmergnerite. Am Mineral 84:333–340.

220 Fritz J, Greshake A, Stoffler D (2005) Micro-Raman spectroscopy of plagioclase and maskelynite in Martian
221 meteorites: evidence of progressive shock metamorphism. Antarct Meteorite Res 18:96–116.

222 Gatta GD (2008) Does porous mean soft? On the elastic behaviour and structural evolution of zeolites under pressure. Z
223 Kristallogr 223:160–170.

224 Gatta GD (2010) Extreme deformation mechanisms in open-framework silicates at high-pressure: Evidence of
225 anomalous inter-tetrahedral angles. Micropor Mesopor Mater 128:78–84.

226 Gatta GD, Lee Y (2014) Zeolites at high pressure: A review. Min Mag 78:267–291.

227 Gatta GD., Lotti P (2016) Cancrinite-group minerals: Crystal-chemical description and properties under non-ambient
228 conditions - A review. Am Mineral 101:253–265.

229 Mao HK, Xu J, Bell PM (1986) Calibration of the ruby pressure gauge to 800 kbar under quasi-hydrostatic conditions. J
230 Geophys Res 91:4673.

231 Miletich R, Allan DR, Kuhs WF (2000) High-pressure single crystal techniques. In: Hazen RM, Downs RT (eds) High-
232 temperature and high-pressure crystal chemistry. Reviews in Mineralogy and Geochemistry. pp 445–519

233 Ohashi Y, Burnham CW (1973) Clinopyroxene Lattice Deformations: The Roles of Chemical Substitution and
234 Temperature. Am Mineral 58:843–849.

235 Tribaudino M, Angel RJ, Cámara F, Nestola F, Pasqual D, Margiolaki I (2010) Thermal expansion of plagioclase
236 feldspars. Contrib to Mineral Petrol 160:899–908.

237 Tribaudino M, Bruno M, Nestola F, Pasqual D, Angel RJ (2011) Thermoelastic and thermodynamic properties of
238 plagioclase feldspars from thermal expansion measurements. Am Mineral 96:992–1002.

239 Velde B, Syono Y, Kikuchi M, Boyer H (1989) Raman microprobe study of synthetic diaplectic plagioclase feldspars.
240 Phys Chem Miner 16:436–441.

241

242 **Tables**

243

244 **Table 1** Raman shifts as a function of pressure for six selected Raman modes

245

			P < 6.5 GPa		P > 6.5 GPa	P > 8.5 GPa	
Modes (cm^{-1})	$\|\Delta\upsilon\|_{0\text{-}10.4\ GPa}$ (cm^{-1})	$\Delta\upsilon/\Delta P$ ($cm^{-1}GPa^{-1}$)	uncertainties ($cm^{-1}GPa^{-1}$)	$\Delta\upsilon/\Delta P$ ($cm^{-1}GPa^{-1}$)	uncertainties ($cm^{-1}GPa^{-1}$)	$\Delta\upsilon/\Delta P$ ($cm^{-1}GPa^{-1}$)	uncertainties ($cm^{-1}GPa^{-1}$)
149	26.0	2.7	0.1				
290	15.7	1.9	0.1	1.3	0.1		
478	29.1	3.6	0.1	1.9	0.3		
507	16.2	1.1	0.1	2.9	0.2		
578	4.2	1.8	0.1	-1.4	0.2		
815	17.3	2.2	0.1	-0.5	0.5	3.1	0.4

246

247 **Caption of the Figures**

248

249 **Fig. 1** Pressure-evolution of the Raman spectrum of low albite during isothermal (T = 25 °C) compression and
250 decompression, from 0.0001 to 10.4 GPa. The spectrum at 0.0001 GPa was collected with the crystal in air

251 **Fig. 2** Pressure-evolution of some selected Raman bands. Full and empty symbols correspond to the compression and
252 decompression experiments, respectively. Lines are least square fits to data, to use as guide to the eye

253 **Fig. 3** Plots of the four possible tilts in the alkali-feldspar structure as a function of pressure. Tilts have been defined
254 and calculated according to Angel et al. (2012). Data from the refinements of Benusa et al. (2005) and the lower-*P*
255 refinements by Downs et al. (1994)

256 **Fig. 4** The shear of the four-membered ring of tetrahedra. O-O-O angles from Benusa et al. (2005); tilt #4 is defined in
257 Angel et al. (2012), along with the protocol for its calculation. Lines are drawn as guide to the eye

258 **Fig. 5** Vibrational patterns of the modes corresponding to the Raman bands at 478, 507, 578 and 815 cm^{-1}, projected on
259 the *ab* plane. Wavenumbers refer to room *T*,*P*. Calculated atomic displacements are indicated as black arrows. Atom
260 types are: Na (yellow), Si (red), Al (green) and O (blue)

261 **Figures**

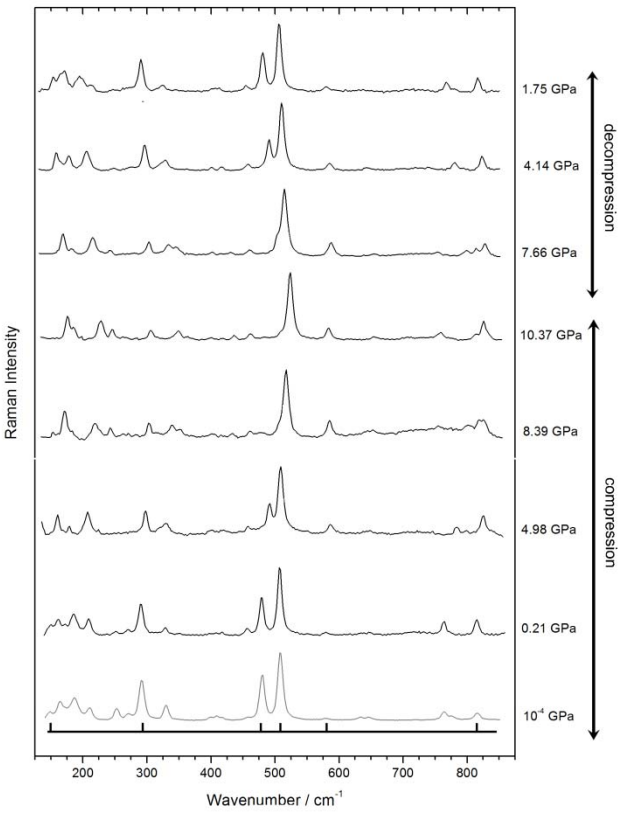

262

263 Fig1.tiff

264 Graphics program: Origin Pro8

265

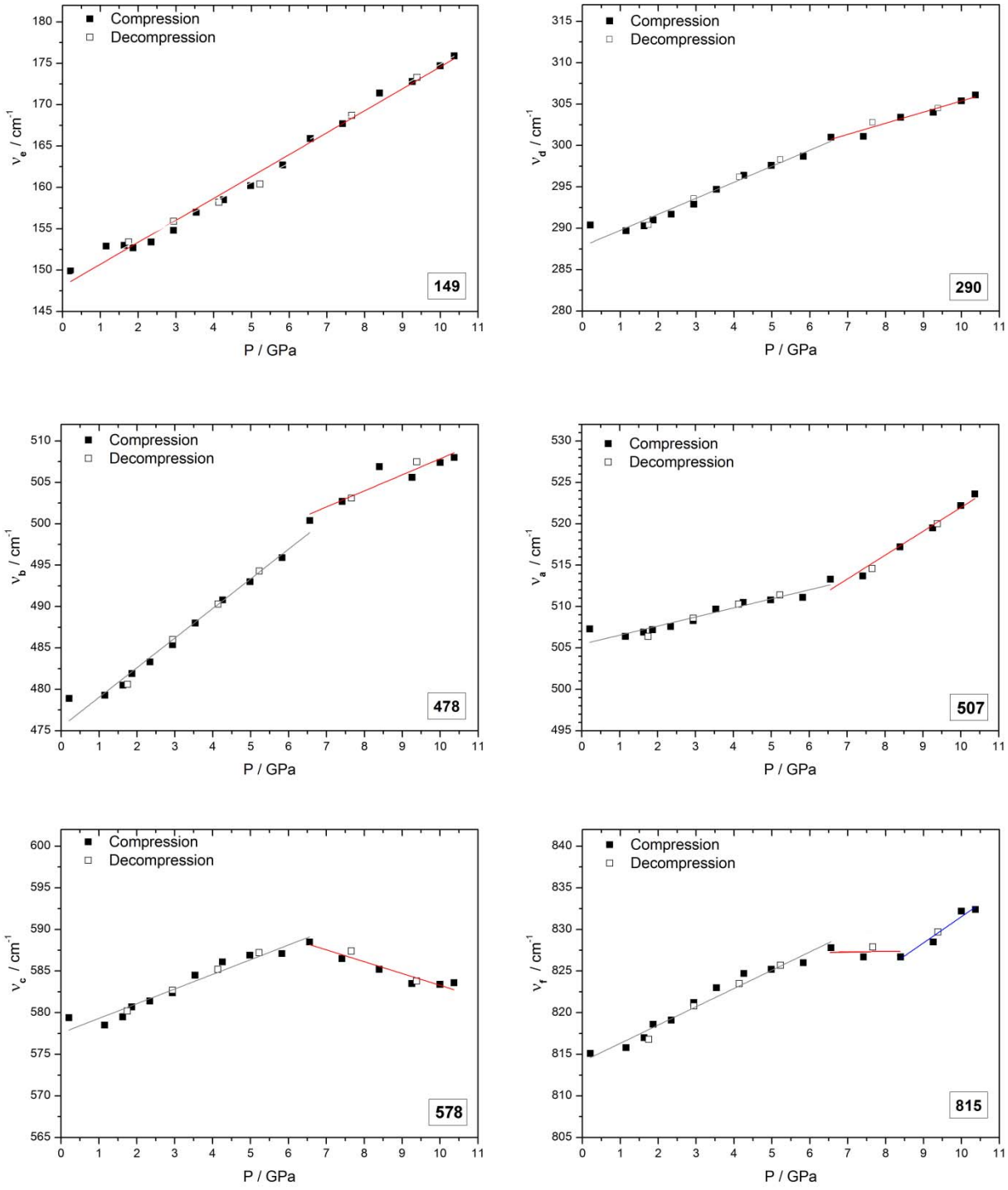

Fig2.tiff

Graphics program: Origin Pro8

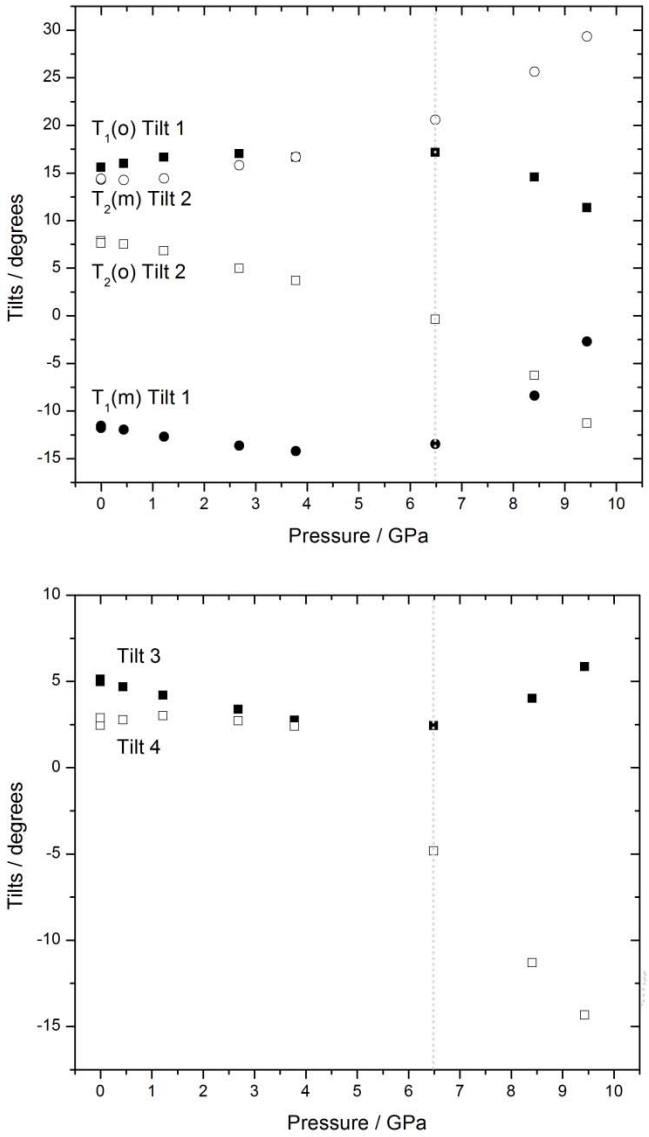

271

272 Fig3.tiff

273 Graphics program: Origin Pro8

274

275

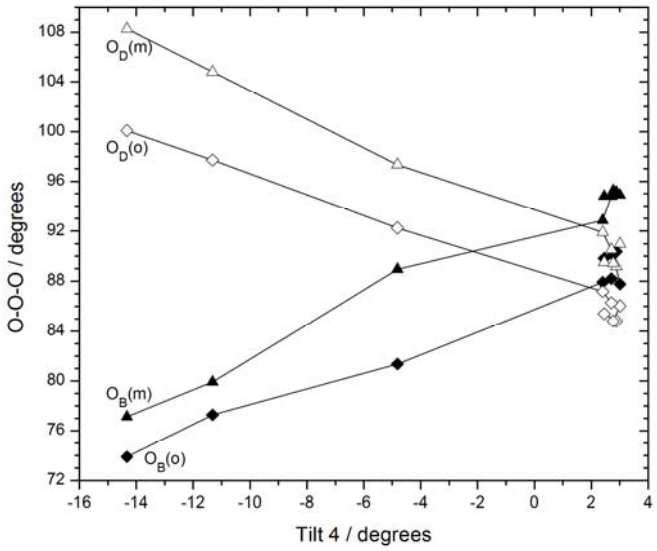

276

277 Fig4.tiff

278 Graphics program: Origin Pro8

279

280

281

282

283

284

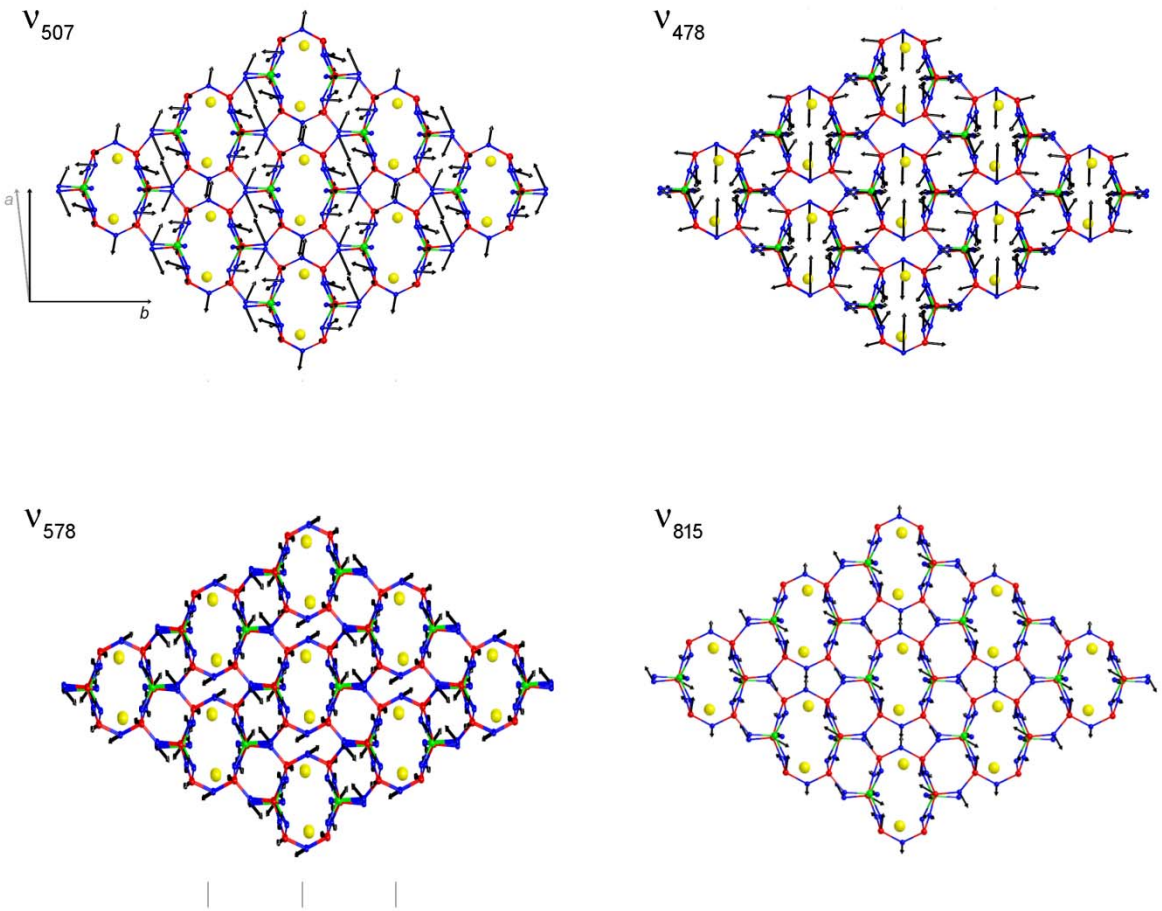

Fig5.tiff

Graphics program: Moldraw software (http://www.moldraw.unito.it)